H$_2$S regulation of ferroptosis attenuates sepsis-induced cardiomyopathy

GUODONG CAO[1,2*], YOUCHENG ZENG[1*], YUHAN ZHAO[1], LIANG LIN[1], XIQING LUO[1],
LICHUN GUO[1], YIXIN ZHANG[1] and QINGHONG CHENG[1,2]

[1]Department of Critical Care Medicine, Medical School of Shihezi University;
[2]The Second Department of Critical Care Medicine, The First Affiliated Hospital, School of Medicine,
Shihezi University, Shihezi, Xinjiang Uyghur Autonomous Region 832000, P.R. China

Abstract. Ferroptosis is a non-apoptotic form of cell death mediated by reactive oxygen species (ROS). Iron metabolism disorders play a key role in sepsis-induced cardiomyopathy (SIC). While hydrogen sulfide (H$_2$S) inhibits SIC, it is unknown if it does so by controlling ferroptosis. The present study evaluated whether sodium hydrosulfide (NaHS), an H$_2$S donor, alleviates SIC by decreasing ferroptosis. Lipopolysaccharide (LPS) was employed to induce an *in vitro* model of septic myocardial injury in rat H9c2 cardiomyocytes. The myocardial injury model of septic rats was established by cecal ligation and puncture (CLP). Cardiomyocyte injury was evaluated using Cell Counting Kit-8 and myocardial enzyme assay and hematoxylin and eosin (H&E) staining. The cardiac function of rats was assessed using echocardiography and changes in myocardial fibers and mitochondria were evaluated using H&E staining and transmission electron microscopy, respectively. Fe^{2+}, glutathione and malondialdehyde levels in cardiomyocytes were detected using assay kits, ROS and mitochondrial membrane potential changes were detected using fluorescent probes and ferroptosis and Beclin 1 (BECN1) signaling pathway-associated protein expression levels were semi-quantified using western blotting. NaHS decreased ferroptosis of H9c2 cells induced by LPS and decreased injury of myocardial cells by improving iron metabolism disorder and oxidative stress levels. Furthermore, *in vivo* results demonstrated that NaHS attenuated CLP-induced septic myocardial ferroptosis and significantly improved cardiac dysfunction in septic rats compared with the CLP group. NaHS was demonstrated to attenuate sepsis-induced myocardial cell and tissue injury by significantly inhibiting the phosphorylation of BECN1 and significantly increasing expression levels of the ferroptosis regulatory proteins solute carrier family 7 member 11 and glutathione peroxidase 4. The results of the present study suggested that by regulating the BECN1 signaling pathway, NaHS may decrease the incidence of myocardial ferroptosis, thereby improving SIC.

Introduction

Sepsis is a potentially fatal condition characterized by systemic organ damage and dysfunction induced by an abnormal host response to infection (1). With the expansion of the 'Save Sepsis' campaign, the international guidelines for sepsis and infectious shock management in 2021 emphasized the role of multi-organ dysfunction, early detection and sepsis treatment (2). The heart is one of the most sensitive organs to sepsis and sepsis-induced cardiomyopathy (SIC) is frequently observed in the intensive care unit, with an incidence of 10-70% in patients with sepsis in the United States (3). The pathophysiology of SIC includes dysregulation of inflammatory mediators, mitochondrial dysfunction, oxidative stress, calcium regulatory abnormality, dysregulation and endothelial dysfunction of the autonomic nervous system, endoplasmic reticulum stress, autophagy and ferroptosis (4,5).

Ferroptosis is a unique form of programmed cell death dependent on reactive oxygen species (ROS) and iron and is distinct from apoptosis, necrosis and autophagy (6). Ferroptosis is primarily caused by a blockage of the cystine/glutamate reverse transporter system x$_c^-$ (system x$_c^-$), oxidative stress, iron overload and lipid peroxidation accumulation. System x$_c^-$ comprises the catalytic subunit solute carrier family 7 member 11 (SLC7A11) and the chaperone subunit solute carrier family 3 member 2 (7); inhibition of system x$_c^-$ transport decreases cellular antioxidant capacity and causes toxic lipid peroxide accumulation, eventually leading to cellular ferroptosis (8). Beclin 1 (BECN1), an endogenous SLC7A11-binding protein, is key for the regulation of ferroptosis (9). Ferroptosis has been associated with diabetic (10), azithromycin-induced (11) and iron overload

Correspondence to: Professor Qinghong Cheng, The Second Department of Critical Care Medicine, The First Affiliated Hospital, School of Medicine, Shihezi University, 107 North Second Road, Shihezi, Xinjiang Uyghur Autonomous Region 832000, P.R. China
E-mail: xunfeicheng@aliyun.com

*Contributed equally

cardiomyopathy (12) and lipopolysaccharide (LPS)-induced acute lung (13) and acute kidney injury (14). However, additional research is required to determine the precise mechanism and therapeutic targets of ferroptosis in LPS- and cecal ligation and puncture (CLP)-induced cardiomyocyte injury in septic rats.

In mammals, H_2S is regarded as the 'third novel medical signaling gas molecule' and serves an important role in protecting cells from oxidative stress and signal transduction (15). H_2S synthesis is dependent on three enzymes: Cystathionine β-synthase, cystathionine γ-lyase and 3-mercaptopyruvate sulfur-transferase (16). H_2S synthesis is implicated in a range of pathological and physiological processes, including inflammation (17), oxidative stress (18), apoptosis (19) and autophagy (20). NaHS has been reported to enhance LPS-induced SIC via regulation of signaling pathways, such as the toll-like receptor 4 pathway, and endoplasmic reticulum stress (21). Although NaHS has been widely investigated in the prevention and treatment of sepsis (22,23), its regulatory mechanisms and involvement in ferroptosis regulation in SIC require further elucidation. In the present study, an *in vitro* model of LPS-induced H9c2 cardiomyocyte injury and an *in vivo* model of CLP-induced sepsis were employed to determine whether the H_2S donor NaHS alleviates septic myocardial injury by decreasing oxidative stress and cardiomyocyte ferroptosis.

Materials and methods

Cell culture and processing. The rat cardiomyocyte H9c2 cell line (Procell Life Science & Technology) was cultured in flasks containing 89% DMEM (Gibco; Thermo Fisher Scientific, Inc.), 10% fetal bovine serum (Gibco; Thermo Fisher Scientific, Inc.) and 1% 10,000 U/ml penicillin-streptomycin (HyClone; Cytiva) at 37˚C under 5% CO_2. The cells were pretreated with NaHS (Sigma-Aldrich; Merck KGaA; 20, 50, 100, 150 and 200 μmol/l) for 1 h at 37˚C prior to cell stimulation with LPS (Sigma-Aldrich; Merck KGaA; 1, 3, 5, 10 and 20 μg/ml) for 24 h at 37˚C. The control group received double-distilled water to the same volume as the experimental group.

Cell viability assay. Cell Counting Kit-8 (CCK-8) assay (cat. no. CK04; Dojindo Laboratories, Inc.) was used to assess cell viability. H9c2 cells were seeded in 96-well plates, at a density of $2x10^4$ cells/well and cultured for 24 h at 37˚C. The cells were pretreated with 20, 50, 100, 150 and 200 μM NaHS for 1 h at 37˚C prior to cell stimulation with 1, 3, 5, 10 and 20 μg/ml LPS for 24 h at 37˚C. Subsequently, 10 μl CCK-8 solution was added to each well and the 96-well plates were incubated for 2 h at 37˚C and the cells were then incubated for 3 h. The optical density was measured at 450 nm using a microplate reader (Thermo Fisher Scientific, Inc.). The cell vitality was calculated as follows: Cell viability (%)=(absorbance of treatment-absorbance of blank)/(absorbance of control-absorbance of blank) x100.

Determination of lactate dehydrogenase (LDH), creatine kinase-myocardial band (CK-MB), glutathione (GSH), malondialdehyde (MDA), Fe^{2+} and ROS levels and mitochondrial membrane potential. H9c2 ($2x10^4$ cells/well) were pre-treated

with 50 μmol/l NaHS for 1 h prior to cell stimulation with 5 μg/ml LPS for 24 h at 37˚C. The cells were separated into three groups as follows: i) Control, ii) LPS and iii) LPS + NaHS. LDH Activity Assay (cat. no. BC0680; Beijing Solarbio Science and Technology Co., Ltd.), CK-MB ELISA (cat. no. SEKM-0152; Beijing Solarbio Science and Technology Co., Ltd.), Reduced GSH Content Assay (cat. no. BC1170; Beijing Solarbio Science and Technology Co., Ltd.), MDA Content Assay (cat. no. BC0020; Beijing Solarbio Science and Technology Co., Ltd.) and Total Iron Content Colorimetric Assay kits (cat. no. E1042; Applygen Technologies, Inc.) were used to evaluate levels each marker in supernatant (4˚C, 200 g, 5 min) according to the manufacturers protocol. The ROS and mitochondrial membrane potential changes in rat H9c2 cardiomyocytes were quantified by measuring the fluorescence of DCFH-DA ROS (cat. no. D6470; Beijing Solarbio Science and Technology Co., Ltd.) and JC-1 (cat. no. J8030; Beijing Solarbio Science and Technology Co., Ltd.) fluorescent probes, respectively. The cells were incubated with DCFH-DA ROS and JC-1 working solution at 37˚C for 30 min. Subsequently, 1X PBS was used to wash cells at least two times. Images were captured under a fluorescence microscope (magnification, x200) and evaluated using ImageJ software (vl46; National Institutes of Health).

Western blotting. Total protein was extracted from H9c2 cells and myocardial tissue using RIPA lysis buffer (cat. no. R0010; Beijing Solarbio Science & Technology Co., Ltd.). Protein concentration was evaluated using a Pierce BCA protein assay kit (cat. no. PC0020; Beijing Solarbio Science & Technology Co., Ltd.). The protein samples (10 μg/lane) were then separated using 10 and 12% SDS-PAGE and electrophoresed. The proteins were electro-transferred onto PVDF membranes. The membranes were blocked with 5% bovine serum albumin (cat. no. A8020; Beijing Solarbio Science & Technology Co., Ltd.) for 2 h at room temperature before overnight incubation at 4˚C with primary antibodies as follows: BECN1 (1:1,000; cat. no. ab210498; Abcam), phosphorylated (p)-BECN1 (1:1,000; cat. no. ab183313; Abcam), GPX4 (1:1,000; cat. no. T56959; Abmart Pharmaceutical Technology Co., Ltd.), SLC7A11 (1:1,000; cat. no. T57046; Abmart Pharmaceutical Technology Co., Ltd.), ferritin (1:1,000; cat. no. T55648 Abmart Pharmaceutical Technology Co., Ltd.) and β actin (1:1,000; cat. no. TA328071; OriGene Technologies, Inc.). After washing the PVDF membranes, the secondary antibodies were incubated for 1 h at room temperature. Secondary antibodies were as follows: Peroxidase Conjugated Affinity Purified Goat anti-Mouse IgG (H+L) (1:10,000; cat. no. TA130003; OriGene Technologies, Inc.) and Goat Anti-Rabbit IgG Secondary Antibody (1:10,000; cat. no. TA130015 OriGene Technologies, Inc.). Gels were washed, incubated with high-sensitivity ECL (cat. no. WBULS0100; Sigma-Aldrich; Merck KGaA) according to manufacturer's protocol and imaged. Band intensity was semi-quantified and evaluated using ImageJ software (vl46; National Institutes of Health).

Immunofluorescence staining. As aforementioned, H9c2 ($2x10^4$ cells/well) were pre-treated with 50 μmol/l NaHS for 1 h prior to cell stimulation with 5 μg/ml LPS for 24 h at 37˚C. Cells were fixed using 4% paraformaldehyde for 24 h at room temperature, blocked with PBS containing 1% BSA

(cat. no. A8020; Beijing Solarbio Science & Technology Co., Ltd.) for 1 h at room temperature, followed by over-night incubation at 4˚C with primary antibodies BECN1 (1:1,000; cat. no. ab210498; Abcam) and SLC7A11 (1:1,000; cat. no. T57046; Abmart Pharmaceutical Technology Co., Ltd.). The next day, cultures were gently washed three times and incubated for 50 min at room temperature with a Cy3 conjugated Goat Anti-Rabbit IgG (H+L) (1:500; cat. no. GB21303; Wuhan Servicebio Technology Co., Ltd.). The nuclei were counterstained with DAPI (cat. no. G1012; Servicebio, Inc.) for 10 min at room temperature and washed three times for 5 min each. The slides were gently shaken before being sealed with Anti-Fluorescence Quenching Sealing Reagent (cat. no. G1401; Servicebio, Inc.) for 10 min at room temperature. Images were captured under a fluorescence microscope (magnification, x200) and evaluated using ImageJ software (v146; National Institutes of Health). Finally, Pearson's correlation coefficient and Mander's co localization coefficient were used to evaluate the expression of fluorescence colocalization using Dunn *et al's* scoring system (24).

BECN1 small interfering (si)RNA transfection. BECN1 fragments and mutants were synthesized by Shanghai GenePharma Co., Ltd. as follows: BECN1-siRNA, 5'-GCG GACAATTTGGCACGATCA-3' and negative control (NC)-siRNA: 5'-TTCTCCGAACGTGTCACGT-3'. The Lentiviral plasmid LV3(H1/GFP&Puro)-BECN1-Rat-1157 was obtained from Shanghai GenePharma Co., Ltd. 293T cells (Shanghai GenePharma Co., Ltd.) were co-transfected with the second-generation lentiviral plasmid (10 μg) and packaging plasmids (pGag/Pol, pRev, PVSV-G), and mixed according to the ratio of 2:1:1:1. Incubated at 37˚C in 5% CO_2 incubator for 48 h. Lentivirus was produced and H9c2 cells were trans-duced for 48 h at 37˚C with 5 μl/well BECN1-siRNA (1 μg/μl) or NC-siRNA, the titer of BECN1-siRNA was determined to be 3×10^8 TU/ml, and the MOI for H9c2 infection was 20. After lentiviral transduction and under the same conditions for 48 h. Then, 10,000 U/ml penicillin-streptomycin was used for maintenance, 5 μg/ml puromycin was used to screen cells and protein expression levels of BECN1 were assessed using western blotting. Following stable transfection, H9c2 cells were treated with 50 μmol/l NaHS for 1 h at 37˚C, then stimulated with 5 μg/ml LPS for 24 h at 37˚C. H9c2 cells were divided into treatment groups as follows: i) LPS; ii) BECN1-siRNA + LPS; iii) LPS + NaHS and iv) BECN1-siRNA + LPS + NaHS.

Animal model. A total of 30 male Sprague-Dawley (SD) rats (age, 6-8 weeks; weight, 200±10 g) was purchased from the Animal Experimentation Center of Xinjiang Medical University [animal license no. SYXK (new) 2011-010101]. All SD rats were housed in the Animal Experimentation Center of Shihezi University according to the standards described by the National Institutes of Health (25). All rats were housed under standard conditions of 25˚C, 60% relative humidity and 12/12-h light/dark cycle with free access to standard labora-tory food and water. The present study was approved by the Institutional Ethics Committee of The Medical Committee of The First Affiliated Hospital of Shihezi University School of Medicine (approval no. A2022-104-01).

Establishment of the SIC model and model grouping. The septic myocardial injury model was established using the previously reported CLP method (26). Briefly, rats were fasted for 12 h before surgery without water restriction. Rats were anesthetized using isoflurane inhalation (induction, 2.5%; maintenance, 1.0%). The abdominal cavity was cut along the midline, the cecum was ligated and the end of the cecum was perforated once with a 50-gauge needle; after squeezing out a small amount of feces, the abdomen was closed. Following surgery, 1 ml/100 g saline was administrated subcutane-ously for resuscitation without diet restriction. Rats in the sham group (n=10) underwent the same surgical procedure without CLP. In the CLP + NaHS group (n=10), 8.9 μmol/kg NaHS was administered by intraperitoneal injection 1 h after CLP (26). All rats in the CLP group demonstrated symptoms such as increased respiratory and heart rate (HR), listlessness, vertical hair, huddling, reduced food intake and decreased activity following CLP modeling, which was consistent with the previously reported rat sepsis model (26,27). At 12 h after surgery, the cardiac function of rats in each group was evaluated using echocardiography. When rats were unable to move, slow to respond and demonstrating symptoms such as diarrhea or urinary incontinence, abdominal infection and suppuration or reached the end of the experimental timeline, i.e. 12 h after the operation. They were anesthetized with isoflurane (induction, 2.5%) and euthanized by cervical dislocation. The death of rats was confirmed by cardiac and respiratory arrest, muscle relaxation and lack of reflex. The myocardial injury was assessed using hematoxylin and eosin (H&E) staining. Changes in myocardial fiber microstructure and mitochondria were evaluated using transmission electron microscopy and myocardial tissue protein was extracted to determine ferroptosis-associated protein expression using western blotting.

Echocardiography. At 12 h after surgery, rats were anesthe-tized using isoflurane (induction, 2.5%; maintenance, 1.0%) and the anterior chest hair was shaved. Rates were placed in the left supine position on the examination table, connected to an electrocardiogram and GE Vivid E9 Ultrasound Machine with 12 sec heart probe and probe frequency 12 Mhz was used to perform echocardiography. HR and left ventricular end-diastolic diameter (LVEDD) were measured under the M-mode ultrasound module and LV ejection fraction (LVEF%) and shortening fraction (LVFS%) were calculated. At least three cardiac cycles were recorded for each rat to reflect the diastolic and systolic functions of the heart.

Histopathological examination. Myocardial tissue specimens from sham, CLP and CLP + NaHS rats were fixed in 4% para-formaldehyde for 24 h at room temperature, paraffin-embedded and cut into 4 μm sections. The tissue sections were stained with H&E for 24 h at room temperature. Subsequently, the tissues were dehydrated in different concentrations of ethanol, embedded in paraffin and sliced into 4-μm-thick sections. The tissue sections were then stained with hematoxylin (0.4%) and eosin (0.1%) (H&E) solution at 37˚C for 5 min and the pathological changes after myocardial injury were observed using a light microscope. Finally, the extent of Pathological

score of myocardial injury was evaluated using the Kishimoto scoring system (28).

Transmission electron microscopy. LV myocardium samples (2x2x2 mm) were collected and fixed in 4% paraformaldehyde and 2.5% glutaraldehyde in 0.1 M phosphate buffer for 2 h at room temperature. Tissue samples were embedded in 1% agarose, the samples were successively dehydrated with 30-50-70-80-95-100-100% alcohol for 20 min each time, and 100% acetone twice for 15 min each time at room temperature and cut into ultrathin sections (70 nm) using an ultramicrotome. Sections were stained using 2% uranyl acetate in pure ethanol for 15 min, followed by 2.6% lead citrate for 15 min at room temperature. At least five images were taken per sample. using a transmission electron microscope (magnification x10,000) at 80 kV. The extent of mitochondrial damage was evaluated using the Flameng scoring system (29).

Statistical analysis. SPSS 26.0 (IBM Corp.) statistical software was used to analyze the data. Data are presented as the mean ± standard deviation. Paired student's t test was used to compare the means of two samples; ≥ 3 samples were compared using one-way ANOVA with complete randomization and post hoc Bonferroni's correction. $P<0.05$ was considered to indicate a statistically significant difference. Each experiment was performed three times.

Results

NaHS attenuates sepsis-induced cardiomyocyte injury and impaired iron metabolism. The effect of LPS and the H_2S donor NaHS on cell viability were assessed to determine the appropriate dose. When LPS concentration increased, H9c2 cell viability significantly decreased and Fe^{2+} concentration significantly increased compared with the control (both $P<0.05$; Fig. 1A and B). When treated with 5 μg/ml LPS, the mean activity of the cell was 50.22% and the concentration of Fe^{2+} released was 140.69% that of the control. These results demonstrated that a SIC model was created using 5 μg/ml LPS. In the LPS-induced myocardial injury model of sepsis in H9c2 cells, NaHS significantly improved the LPS-induced decrease in cell viability for concentrations ≤ 150 μmol/ml and significantly decreased intracellular Fe^{2+} concentration compared with the LPS group (both $P<0.05$; Fig. 1C and D). These data demonstrated that NaHS treatment improved cell viability, decreased cell injury and regulated impaired iron metabolism. However, its effects were independent of concentration. Cell viability was decreased when NaHS concentration was ≥ 100 μmol/l. NaHS at 50 μmol/l produced the greatest treatment effect, therefore it was used in subsequent tests.

JC-1 staining demonstrated that mitochondrial JC-1 polymer (red fluorescence) decreased and JC-1 monomer (green fluorescence) increased in the LPS group, with the red:green ratio significantly decreased compared with the control ($P<0.05$; Fig. 1E). This demonstrated that the mitochondrial membrane potential was decreased, which suggested increased cell damage. Treatment with NaHS significantly reversed this phenomenon ($P<0.05$) compared with the LPS group and demonstrated increased mitochondrial membrane potential level, which suggested that cellular damage was

alleviated. These data indicate that NaHS improves cardiomyocyte viability and alleviates LPS induced iron metabolism disorder and mitochondrial membrane potential abnormality.

NaHS decreases sepsis-induced oxidative stress and lipid peroxidation in cardiomyocytes. Significantly elevated release of cardiac enzymes LDH and CK-MB from H9c2 cells was observed in the LPS group compared with the control ($P<0.05$; Fig. 2A and B), which suggested increased cardiomyocyte injury. NaHS intervention significantly decreased levels of LDH and CK-MB compared with the LPS group ($P<0.05$), which suggested NaHS attenuated cell injury. Following LPS stimulation, the antioxidant GSH activity of H9c2 cells was significantly decreased compared (Fig. 2C), whereas the lipid peroxide MDA content significantly increased compared with the control (both $P<0.05$; Fig. 2D). Furthermore, green fluorescence (indicating ROS) was significantly enhanced in the LPS group compared with the control ($P<0.05$; Fig. 2E), which suggested an imbalance between oxidative and antioxidant effects in cardiomyocytes in response to LPS stimulation and oxidative stress. Following NaHS treatment, GSH activity significantly increased, MDA concentration significantly decreased and ROS fluorescence intensity significantly decreased compared with the LPS group (both $P<0.05$; Fig. 2C, D and E). These data suggested that NaHS enhanced intracellular antioxidant capacity and mitigated oxidative stress and lipid peroxidation caused by LPS in cardiomyocytes.

NaHS inhibits sepsis-induced ferroptosis in cardiomyocytes. Expression levels of the ferroptosis regulatory proteins SLC7A11 and GPX4 were significantly lower, whereas p-BECN1 expression was significantly higher, in the LPS group compared with the control ($P<0.05$; Fig. 3A). NaHS treatment significantly increased SLC7A11 and GPX4 protein expression levels, whereas p-BECN1 protein expression levels were significantly decreased compared with the LPS group ($P<0.05$). Immunofluorescence demonstrated that co-localization characterization parameters, such as Pearson's correlation coefficient and Mander's co-localization coefficient, were significantly elevated following LPS stimulation ($P<0.05$; Fig. 3B). BECN1 co-localization with SLC7A11, a key component of system x_c^-, compared with the control group, the co-localization of BECN1 and SLC7A11 was enhanced after LPS intervention. However, NaHS markedly reversed this effect compared with the LPS group ($P<0.05$). These results suggest that sodium thiohydride alleviates LPS induced ferroptosis in cardiomyocytes by inhibiting the interaction of BECN1 with SLC7A11.

Inhibition of BECN1 expression by NaHS attenuates ferroptosis in cardiomyocytes. The aforementioned data suggested that NaHS may decrease LPS-induced ferroptosis in H9c2 cardiomyocytes via the BECN1/SLC7A11 signaling pathway. To evaluate the association between the BECN1 signaling pathway and ferroptosis, rat H9c2 cardiomyocytes were transfected with siRNA to silence BECN1. The transfected cells were treated with 5 μg/ml LPS and 50 μmol/l NaHS alone or in combination for 24 h. The protein expression levels of BECN1 were significantly reduced in BECN-siRNA compared
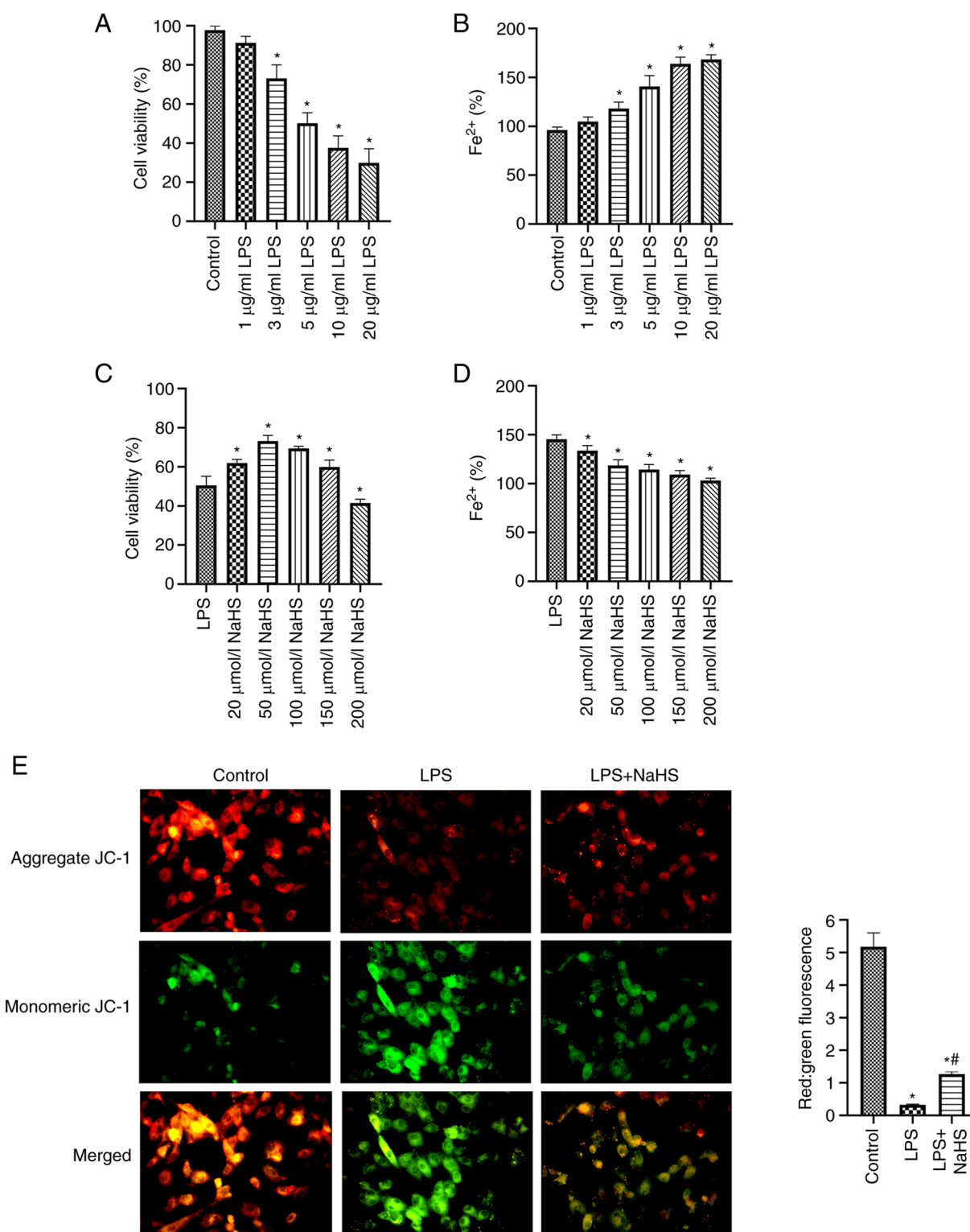
Figure 1. NaHS attenuates sepsis-induced cardiomyocyte injury and impaired iron metabolism. (A) H9c2 cell viability and (B) Fe^{2+} concentration under different concentrations of LPS stimulation. (C) H9c2 cell viability and (D) Fe^{2+} concentration following NaHS intervention with 5 µg/ml LPS stimulation. (E) Aggregate JC-1/Monomeric JC-1 in H9c2 cells (magnification, x200) with 5 µg/ml LPS and 50 µmol/l NaHS. *P<0.05 vs. control; #P<0.05 vs. LPS 5 µg/ml. LPS, lipopolysaccharide; NaHS, sodium hydrosulfide.

with NC-siRNA (P<0.05; Fig. 4A). Therefore, GPX4 protein expression reflects the occurrence of ferroptosis. GPX4 and SLC7A11 protein expression levels were significantly higher and BECN1 protein expression level was decreased in the BECN1-siRNA + LPS group compared with the LPS group (P<0.05; Fig. 4C). Furthermore, ferritin, GPX4 and SLC7A11

protein expression levels were significantly increased and BECN1 protein expression level was significantly decreased in the BECN1-siRNA + LPS + NaHS group compared with the LPS + NaHS group (P<0.05; Fig. 4C). These results suggested that inhibiting BECN1 boosted cells antioxidant capacity and decreased LPS-induced ferroptosis sensitivity in H9c2 cells,
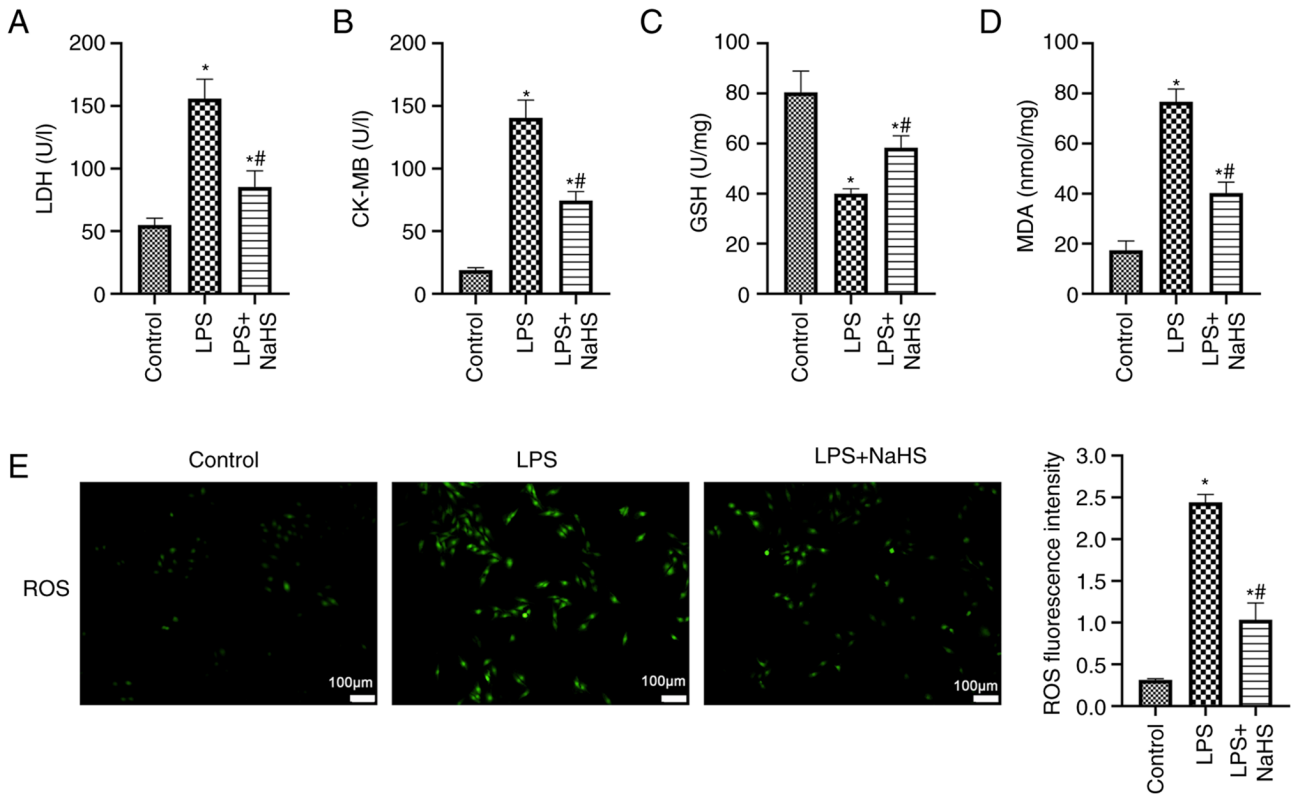
Figure 2. NaHS attenuates sepsis-induced oxidative stress and lipid peroxidation in cardiomyocytes. Levels of cardiac enzymes (A) LDH and (B) CK-MB, (C) GSH, (D) MDA and (E) ROS in H9c2 cells with 5 µg/ml LPS and 50 µmol/l NaHS. *P<0.05 vs. control; #P<0.05 vs. LPS. LPS, lipopolysaccharide; NaHS, sodium hydrosulfide; LDH, lactate dehydrogenase; CK-MB, creatine kinase-myocardial band; GSH, glutathione; MDA, malondialdehyde; ROS, reactive oxygen species.

which indicated BECN1 may serve as a regulator of system x_c^-. NaHS may protect against LPS-induced ferroptosis in H9c2 cells by disrupting the BECN1/SLC7A11 signaling pathway.

NaHS inhibits myocardial ferroptosis and improves SIC. The effect of NaHS on ferroptosis in septic rat heart tissue was assessed using a CLP-induced *in vivo* model of septic myocardial injury. Compared with the sham group, the LVEF%, LVFS% and HR significantly decreased and LVEED significantly increased, and the systolic and diastolic functions of sepsis rats were decreased in the CLP group (P<0.05; Fig. 5A). However, LVEF%, LVFS% and HR significantly increased and LVEDD significantly decreased in the CLP + NaHS group compared with the CLP group (P<0.05). There were no pathological alterations visually apparent in the sham group (Fig. 5B). However, myocardial fibers in the CLP group were misaligned and partially deteriorated compared with the sham group, demonstrating inflammatory cell infiltration, interstitial edema, transverse blurring and erythrocyte exudation, which resulted in significantly higher pathological score (P=0.0017). Myocardial myofilaments in the CLP + NaHS group were more structured than in the CLP group, with no inflammatory infiltration or erythrocyte exudation, Pathological score decreased (P=0.0285). The CLP group exhibited disorganized mitochondrial arrangement, swelling, degeneration, small size and increased density of mitochondria, decreased size and breakage of cristae, partial dissolution and disappearance of the outer membrane, which resulted in significantly increased pathological score significantly higher (P=0.0009;

Fig. 5C) when assessed using transmission electron microscopy. The CLP + NaHS group demonstrated less myocardial mitochondrial damage and more intact membrane compared with the CLP group. However, mitochondrial cristae fractures and swelling remained and the myocardial fibers were more precisely aligned, Pathological score decreased (P=0.0023). Protein expression levels of SLC7A11, GPX4, BECN1 and p-BECN1 were semi-quantified using western blotting in cardiac tissue from rats in each treatment group (Fig. 5D). SLC7A11, GPX4 and ferritin protein expression levels were significantly lowered and p-BECN1 protein expression levels were significantly elevated in the CLP group compared with the sham (P<0.05), which demonstrated activation of ferroptosis. However, NaHS significantly promoted GPX4, SLC7A11 and ferritin protein expression levels and significantly decreased p-BECN1 protein expression levels compared with the CLP group (P<0.05). These results suggested that NaHS-mediated upregulation of SLC7A11 and GPX4 and downregulation of p-BECN1 protected against ferroptosis during SIC.

Discussion

Sepsis is a global health concern that continues to be the leading cause of infection-associated death (30). A recent study reported that septic myocardial injury is associated with increased risk of short- and long-term death from septic shock and that this risk increases with cardiac dysfunction (31). LPS is an integral component of gram-negative bacteria outer membranes that induces systemic inflammatory reactions,
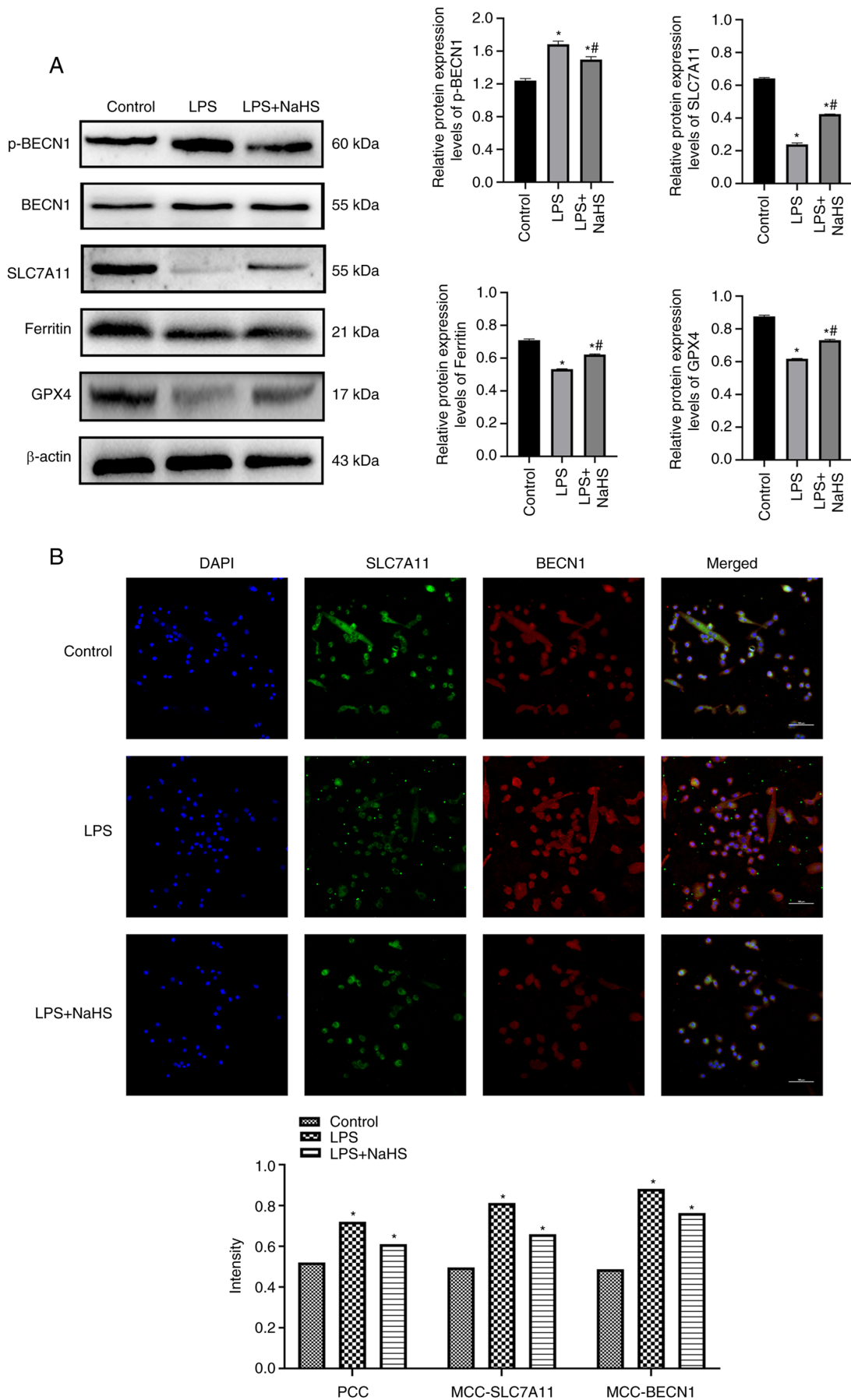
Figure 3. NaHS inhibits sepsis-induced ferroptosis in cardiomyocytes. (A) Ferroptosis regulatory protein expression levels and (B) fluorescence co-localization of BECN1 and SLC7A11 in H9c2 cells treated with 5 µg/ml LPS and 50 µmol/l NaHS. *P<0.05 vs. control; #P<0.05 vs. LPS. LPS, lipopolysaccharide; NaHS, sodium hydrosulfide; BECN1, Beclin 1; SLC7A11, solute carrier family 7 member 11; PCC, Pearson's correlation coefficient; MCC, Mander's co-localization coefficient; GPX4, glutathione peroxidase 4; p-, phosphorylated.
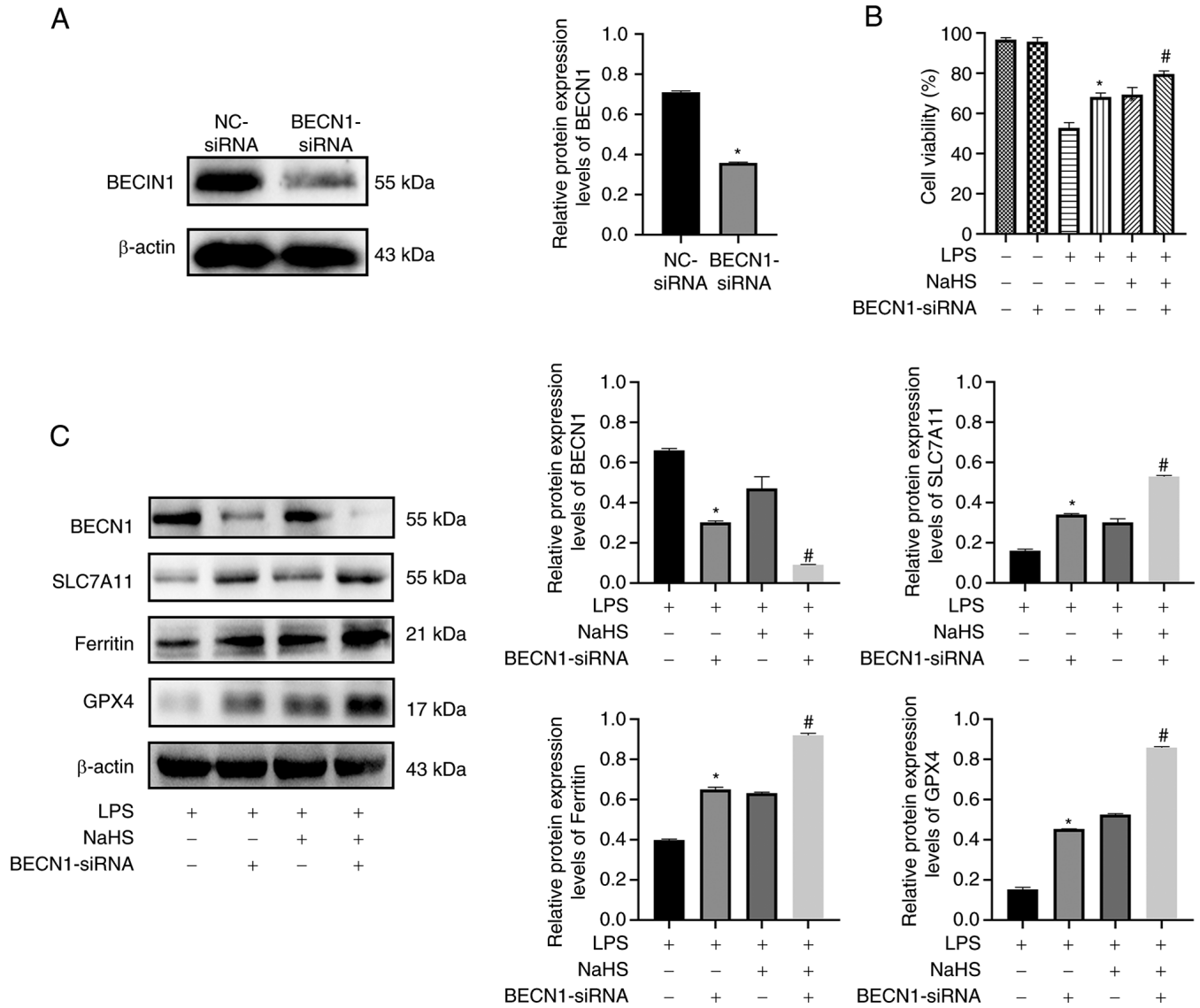
Figure 4. Inhibition of BECN1 expression by NaHS attenuates ferroptosis in cardiomyocytes. (A) Western blotting of BECN1 protein expression levels in BECN1-knockdown cells. (B) Viability of BECN1-knockdown cells following induction with 5 µg/ml LPS. (C) Western blotting of ferroptosis- and BECN1/SLC7A11 signaling-associated protein expression levels in H9c2 cells. *P<0.05 vs. LPS; #P<0.05 vs. LPS + NaHS. LPS, lipopolysaccharide; NaHS, sodium hydrosulfide; BECN1, Beclin 1; si, small interfering; NC, negative control; SLC7A11, solute carrier family 7 member 11; GPX4, glutathione peroxidase 4.

sepsis, infectious shock and multi-organ failure by infiltrating the lymphatic and circulatory systems (32). Myocardial cell injury is the most commonly utilized model of SIC (33). H$_2$S has been reported in substantial basic research to be involved in controlling homeostasis, cardiac contraction, anti-inflammatory, pro-apoptotic and other pathological functions (34-38).

NaHS is a conventional and stable H$_2$S donor with anti-inflammatory, anti-oxidative stress, anti-apoptotic and autophagy-regulating properties (39). It has emerged as a target for sepsis therapeutic research due to its reported regulation of AMPK/mTOR and PI3K/Akt/mTOR pathways to decrease sepsis multi-organ injury (27,40). To the best of our knowledge, however, the role of NaHS in SIC and its mechanisms have not been elucidated. To study the protective effect of NaHS on SIC, LPS was used in the present study to induce rat H9c2 cardiomyocytes to produce an *in vitro* model of sepsis myocardial injury; a CLP-induced *in vivo* model of sepsis rat myocardial injury was also used. The present study demonstrated that 50 µmol/l

NaHS decreased the decrease in cell viability caused by LPS stimulation and significantly decreased release of cardiac enzymes compared, thereby minimizing myocardial cell injury *in vitro*. *In vivo* assessments demonstrated that NaHS pretreatment improved cardiac systolic and diastolic dysfunction in septic rats and decreased cardiac tissue degradation, edema and release of inflammatory cells following CLP surgery, which significantly improved myocardial histopathology scores.

Ferroptosis is a new type of cell death in which iron-dependent lipid peroxidation co-exists with oxidative stress (41). GSH, the primary non-enzymatic antioxidant in cells, is a condensed form of glutamate, cysteine and glycine with direct antioxidant effects and serves as a synthetic substrate for GPX4 (42,43). ROS are created by normal cellular physiological processes and are key for biological signaling and cellular balance (44,45). MDA activity, a byproduct of lipid peroxidation, represents the severity of oxygen radical damage to body tissue and is also associated with ferroptosis (46). Oxidative stress and lipid
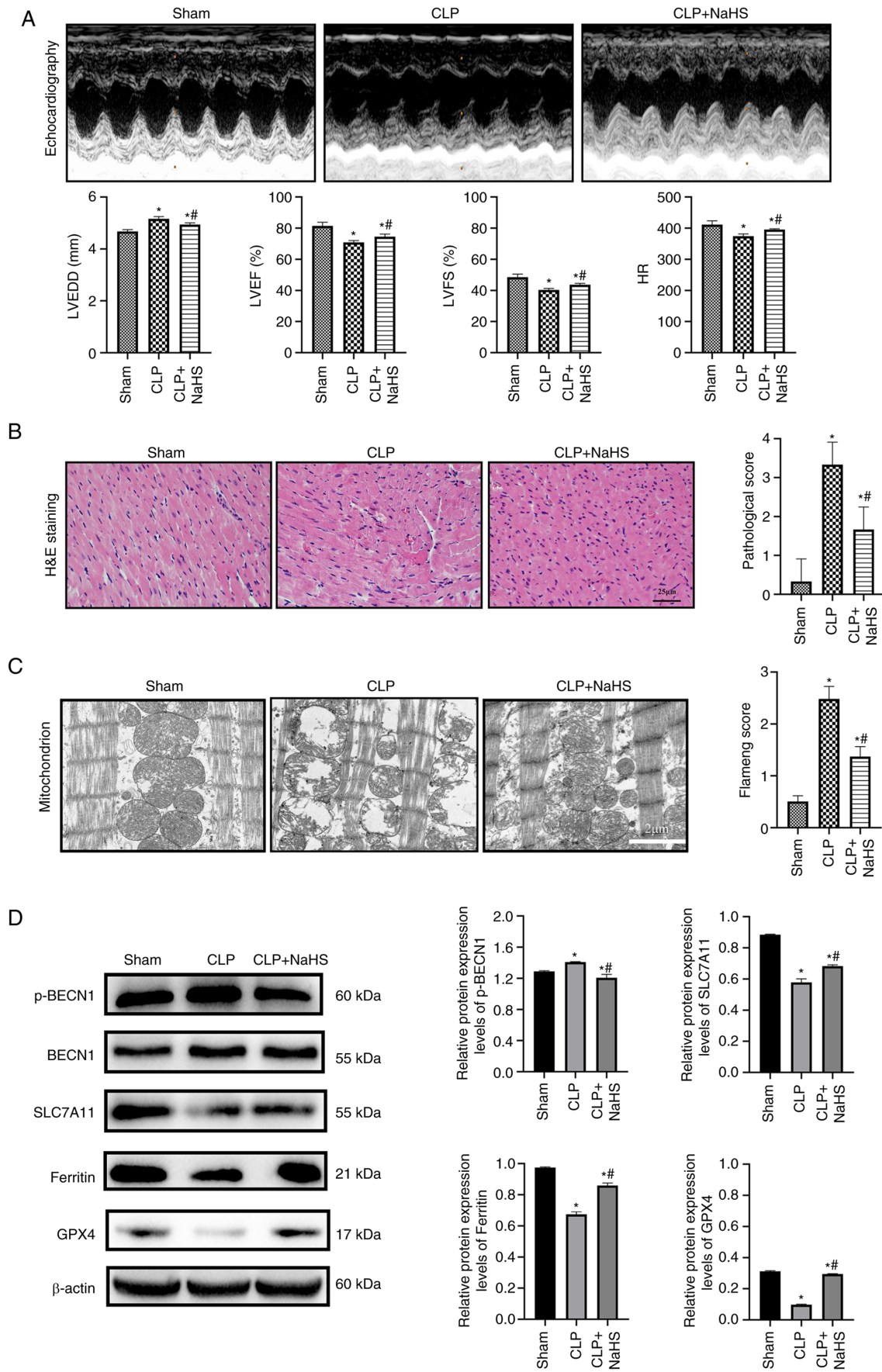
Figure 5. NaHS inhibits myocardial ferroptosis and improves sepsis-induced cardiomyopathy. (A) Cardiac ultrasound and cardiac function index. (B) Representative images of H&E staining of rat myocardial sections. (C) Representative images of mitochondrial transmission electron microscopy of rat myocardium. (D) Western blotting of ferroptosis- and BECN1/SLC7A11 signaling-associated protein expression levels in rat myocardial tissue. *P<0.05 vs. Sham; $^#$P<0.05 vs. CLP. H&E, hematoxylin and eosin; CLP, cecal ligation and puncture; NaHS, sodium hydrosulfide; BECN1, Beclin 1; SLC7A11, solute carrier family 7 member 11; GPX4, glutathione peroxidase 4; p-, phosphorylated.

peroxidation are important in the pathophysiology of myocardial injury and ferroptosis has recently been reported to be a key element in SIC, with suppression of LPS-induced ferroptosis in cardiac tissue alleviating SIC (41). H_2S decreases ferroptosis in acute lung injury by raising protein expression of GPX4 and SLC7A11 in rat lung tissue following CLP surgery and prevented autophagy activation in acute lung injury via blocking the mTOR signaling pathway (47). The involvement of NaHS in CLP-induced myocardial ferroptosis is uncertain. The present study demonstrated that MDA levels rose significantly following LPS stimulation compared with the control, which suggested that lipid peroxidation was involved in this model of cardiac cell injury. In combination with significantly decreased GSH activity and GPX4 and SLC7A11 protein expression levels following LPS treatment, these data suggested that ferroptosis-induced oxidative stress and lipid peroxidation were involved in the development of SIC. When treated with NaHS, the levels of antioxidant marker GSH increased and the lipid peroxidation product MDA was significantly decreased compared with the LPS group. These data demonstrated that NaHS protected against septic myocardial damage by decreasing oxidative stress and lipid peroxidation in the heart.

Ferroptosis is an iron-dependent form of programmed cell death characterized by lipid peroxidation and morphological alteration (48). Ferritin, an iron storage protein, is key in iron metabolism because it stores and releases iron to maintain iron homeostasis in the body. Iron homeostasis has been reported to be critical for normal heart function (49). Iron shortage and overload are linked to cardiomyopathy and heart failure via SLC7A11 pathway (50). When intracellular Fe^{2+} levels rise, the body produces large amounts of hydroxyl radicals and ROS, both of which are harmful to cells, via the Fenton reaction, worsening the occurrence of ferroptosis (51). LPS induces ferroptosis by activating cardiomyocyte nuclear receptor coactivator 4 (NCOA4), which increases its expression. NCOA4 interacts directly with ferritin to degrade it, releasing large amounts of Fe^{2+} and inducing excessive mitochondrial ROS production (52). Aberrant changes in mitochondrial membrane potential are not only key signs of mitochondrial damage and ferroptosis initiation but also an early warning of the occurrence of ferroptosis (53). The present study demonstrated a significant increase in Fe^{2+} content and significantly decreased mitochondrial membrane potential and ferritin protein expression levels in cells following LPS stimulation compared with the control. Following CLP, transmission electron microscopy of cardiac tissue demonstrated disrupted mitochondrial organization, swelling, degeneration of mitochondria and decreased and fragmented cristae. The present study demonstrated that NaHS administration significantly improved iron metabolism in myocardial cells and tissue compared with the LPS group, which suggested that NaHS decreased ferroptosis in septic myocardial injury.

BECN1 is a key regulator of autophagy and has been reported in the pathophysiology of diseases such as metabolic disorders and tumors (54,55). In sepsis, cardiac dysfunction is a key cause of multi-organ dysfunction and BECN1-dependent autophagy has been reported to protect the heart (56,57). However, the regulatory mechanisms governing BECN1 and autophagy remain unclear. Song *et al* (58) reported a potential mechanism by which BECN1 may enhance ferroptosis in cancer cells via modulation of system x_c^- activity, thereby enhancing GSH depletion and lipid peroxidation. This mechanism is dependent on formation of the BECN1-SLC7A11 complex (58). BECN1 regulates ferroptosis independently of autophagy, as reported by previous studies (59,60). Liu *et al* (60) reported that BECN1 overexpression aggravates isoflurane-induced cell damage via upregulation of ferroptosis. This effect is significantly attenuated by silencing of BECN1 in SH-SY5Y cells. Liu *et al* suggested that BECN1 may regulate ferroptosis via inhibition of the glutamate exchange activity of system x_c^-, which is involved in isoflurane-induced toxicity (60). These results are similar to the present study, which demonstrated that LPS significantly increased the phosphorylation of BECN1 while significantly decreasing the protein expression levels of SLC7A11, a core component of system x_c^- compared with the control. Furthermore, immunofluorescence staining demonstrated significantly enhanced co-localization of BECN1 and SLC7A11, which form a BECN1-SLC7A11 complex, decreasing system x_c^- activity and thus regulating ferroptosis (58). BECN1 knockdown decreased LPS-induced cell damage, which in turn prevented ferroptosis. When cells were treated with NaHS, a significant decrease in p-BECN1 and significant increase in SLC7A11 protein expression levels were observed compared with the LPS group. Furthermore, inhibiting BECN1 expression markedly diminished the protective effect of NaHS on H9c2 cells. It could therefore be hypothesized that BECN1 acts as a key signaling component in the transition between autophagy and ferroptosis in septic cardiac damage. However, there is a close relationship between ferroptosis and autophagy, BECN1 knockout mice were not used in animal experiments, the precise chemical mechanism of this action requires further study. Evaluation of the use of NaHS in sepsis multi-organ dysfunction based on autophagy and ferroptosis requires further study.

In conclusion, the present study demonstrated that NaHS alleviated SIC via modulation of the BECN1 signaling pathway, decreased oxidative stress and lipid peroxidation levels and inhibition of ferroptosis. Ferroptosis is predicted to be a novel therapeutic target for SIC and NaHS may be an effective treatment for SIC.

Availability of data and materials

The datasets used and/or analyzed during the current study are available from the corresponding author on reasonable request.

Authors' contributions

QC, GC and YCZ conceived and designed the present study and wrote and revised the manuscript. GC, YCZ and YHZ

wrote the manuscript and analyzed the data. GC, YHZ, LL and XL performed cell experiments and collected data. YCZ, LG and YXZ reviewed the literature and performed animal experiments. GC, YCZ, LG, XL and YXZ analyzed and interpreted the data and produced the figures. All authors have read and approved the final manuscript. QC and GC confirm the authenticity of all the raw data.

Ethics approval and consent to participate

The present study was approved by the Institutional Ethics Committee of The Medical Committee of The First Affiliated Hospital of Shihezi University School of Medicine (approval no. A2022-104-01).

Patient consent for publication

Not applicable.

Competing interests

The authors declare that they have no competing interests.

References

1. Shankar-Hari M, Phillips GS, Levy ML, Seymour CW, Liu VX, Deutschman CS, Angus DC, Rubenfeld GD and Singer M; Sepsis Definitions Task Force: Developing a new definition and assessing new clinical criteria for septic shock: For the third international consensus definitions for sepsis and septic shock (sepsis-3). JAMA 315: 775-787, 2016.
2. Evans L, Rhodes A, Alhazzani W, Antonelli M, Coopersmith CM, French C, Machado FR, Mcintyre L, Ostermann M, Prescott HC, et al: Surviving sepsis campaign: International guidelines for management of sepsis and septic shock 2021. Intensive Care Med 47: 1181-1247, 2021.
3. Beesley SJ, Weber G, Sarge T, Nikravan S, Grissom CK, Lanspa MJ, Shahul S and Brown SM: Septic cardiomyopathy. Crit Care Med 46: 625-634, 2018.
4. Hollenberg SM and Singer M: Pathophysiology of sepsis-induced cardiomyopathy. Nat Rev Cardiol 18: 424-434, 2021.
5. Fang X, Wang H, Han D, Xie E, Yang X, Wei J, Gu S, Gao F, Zhu N, Yin X, et al: Ferroptosis as a target for protection against cardiomyopathy. Proc Natl Acad Sci USA 116: 2672-2680, 2019.
6. Dixon SJ, Lemberg KM, Lamprecht MR, Skouta R, Zaitsev EM, Gleason CE, Patel DN, Bauer AJ, Cantley AM, Yang WS, et al: Ferroptosis: An iron-dependent form of nonapoptotic cell death. Cell 149: 1060-1072, 2021.
7. Koppula P, Zhuang L and Gan B: Cystine transporter SLC7A11/xCT in cancer: Ferroptosis, nutrient dependency, and cancer therapy. Protein Cell 12: 599-620, 2021.
8. Zhang X, Zheng C, Gao Z, Chen H, Li K, Wang L, Zheng Y, Li C, Zhang H, Gong M, et al: SLC7A11/xCT prevents cardiac hypertrophy by inhibiting ferroptosis. Cardiovasc Drugs Ther 36: 437-447, 2022.
9. Zheng J and Conrad M: The metabolic underpinnings of ferroptosis. Cell Metab 32: 920-937, 2020.
10. Ge ZD, Lian Q, Mao X and Xia Z: Current Status and challenges of NRF2 as a potential therapeutic target for diabetic cardiomyopathy. Int Heart J 60: 512-520, 2019.
11. Zhang H, Wang Z, Liu Z, Du K and Lu X: Protective effects of dexazoxane on rat ferroptosis in doxorubicin-induced cardiomyopathy through regulating HMGB1. Front Cardiovasc Med 8: 685434, 2021.
12. Khamseekaew J, Kumfu S, Wongjaikam S, Kerdphoo S, Jaiwongkam T, Srichairatanakool S, Fucharoen S, Chattipakorn SC and Chattipakorn N: Effects of iron overload, an iron chelator and a T-type calcium channel blocker on cardiac mitochondrial biogenesis and mitochondrial dynamics in thalassemic mice. Eur J Pharmacol 799: 118-127, 2017.
13. Liu P, Feng Y, Li H, Chen X, Wang G, Xu S, Li Y and Zhao L: Ferrostatin-1 alleviates lipopolysaccharide-induced acute lung injury via inhibiting ferroptosis. Cell Mol Biol Lett 25: 10, 2020.
14. Belavgeni A, Meyer C, Stumpf J, Hugo C and Linkermann A: Ferroptosis and necroptosis in the kidney. Cell Chem Biol 27: 448-462, 2020.
15. Kimura H, Nagai Y, Umemura K and Kimura Y: Physiological roles of hydrogen sulfide: Synaptic modulation, neuroprotection, and smooth muscle relaxation. Antioxid Redox Signal 7: 795-803, 2005.
16. Guo W, Cheng ZY and Zhu YZ: Hydrogen sulfide and translational medicine. Acta Pharmacol Sin 34: 1284-1291, 2013.
17. Bhatia M and Gaddam RR: Hydrogen sulfide in inflammation: A novel mediator and therapeutic target. Antioxid Redox Signal 34: 1368-1377, 2021.
18. Yang R, Teng X, Li H, Xue HM, Guo Q, Xiao L and Wu YM: Hydrogen sulfide improves vascular calcification in rats by inhibiting endoplasmic reticulum stress. Oxid Med Cell Longev 2016: 9095242, 2016.
19. Sen N, Paul BD, Gadalla MM, Mustafa AK, Sen T, Xu R, Kim S and Snyder SH: Hydrogen sulfide-linked sulfhydration of NF-κB mediates its antiapoptotic actions. Mol Cell 45: 13-24, 2012.
20. Gotor C, García I, Crespo JL and Romero LC: Sulfide as a signaling molecule in autophagy. Autophagy 9: 609-611, 2013.
21. Chen YH, Teng X, Hu ZJ, Tian DY, Jin S and Wu YM: Hydrogen sulfide attenuated sepsis-induced myocardial dysfunction through TLR4 pathway and endoplasmic reticulum stress. Front Physiol 12: 653601, 2021.
22. Liang D, Huang A, Jin Y, Lin M, Xia X, Chen X and Huang A: Protective effects of exogenous NaHS against sepsis-induced myocardial mitochondrial injury by enhancing the PGC-1α/NRF2 pathway and mitochondrial biosynthesis in mice. Am J Transl Res 10: 1422-1430, 2018.
23. Li T, Zhao J, Miao S, Chen Y, Xu Y and Liu Y: Protective effect of H₂S on LPS-induced AKI by promoting autophagy. Mol Med Rep 25: 96, 2022.
24. Dunn KW, Kamocka MM and McDonald JH: A practical guide to evaluating colocalization in biological microscopy. Am J Physiol Cell Physiol 300: C723-C742, 2011.
25. Hollands C: The animals (scientific procedures) Act 1986. Lancet 2: 32-33, 1986.
26. Li X, Cheng Q, Li J, He Y, Tian P and Xu C: Significance of hydrogen sulfide in sepsis-induced myocardial injury in rats. Exp Ther Med 14: 2153-2161, 2017.
27. Zhao Y and Cheng Q: Exogenous H₂S protects against septic cardiomyopathy by inhibiting autophagy through the AMPK/mTOR pathway. Contrast Media Mol Imaging 2022: 8464082, 2022.
28. Kishimoto C, Kawamata H, Sakai S, Shinohara H and Ochiai H: Enhanced production of macrophage inflammatory protein 2 (MIP-2) by in vitro and in vivo infections with encephalomyocarditis virus and modulation of myocarditis with an antibody against MIP-2. J Virol 75: 1294-1300, 2001.
29. Flameng W, Borgers M, Daenen W and Stalpaert G: Ultrastructural and cytochemical correlates of myocardial protection by cardiac hypothermia in man. J Thorac Cardiovasc Surg 79: 413-424, 1980.
30. Baghela A, Pena OM, Lee AH, Baquir B, Falsafi R, An A, Farmer SW, Hurlburt A, Mondragon-Cardona A, Rivera JD, et al: Predicting sepsis severity at first clinical presentation: The role of endotypes and mechanistic signatures. EBioMedicine 75: 103776, 2022.
31. Vallabhajosyula S, Shankar A, Vojjini R, Cheungpasitporn W, Sundaragiri PR, DuBrock HM, Sekiguchi H, Frantz RP, Cajigas HR, Kane GC and Oh JK: Impact of right ventricular dysfunction on short-term and long-term mortality in sepsis: A meta-analysis of 1,373 patients. Chest 159: 2254-2263, 2021.
32. Dickson K and Lehmann C: Inflammatory response to different toxins in experimental sepsis models. Int J Mol Sci 20: 4341, 2019.
33. Hao R, Su G, Sun X, Kong X, Zhu C and Su G: Adiponectin attenuates lipopolysaccharide-induced cell injury of H9c2 cells by regulating AMPK pathway. Acta Biochim Biophys Sin (Shanghai) 51: 168-177, 2019.
34. Wang Y, Wang S, Xin Y, Zhang J, Wang S, Yang Z and Liu C: Hydrogen sulfide alleviates the anxiety-like and depressive-like behaviors of type 1 diabetic mice via inhibiting inflammation and ferroptosis. Life Sci 278: 119551, 2021.
35. Kabil O and Banerjee R: Enzymology of H2S biogenesis, decay and signaling. Antioxid Redox Signal 20: 770-782, 2014.

36. Zhang Z, Jin S, Teng X, Duan X, Chen Y and Wu Y: Hydrogen sulfide attenuates cardiac injury in takotsubo cardiomyopathy by alleviating oxidative stress. Nitric Oxide 67: 10-25, 2017.
37. Wallace JL, Blackler RW, Chan MV, Da Silva GJ, Elsheikh W, Flannigan KL, Gamaniek I, Manko A, Wang L, Motta JP and Buret AG: Anti-inflammatory and cytoprotective actions of hydrogen sulfide: Translation to therapeutics. Antioxid Redox Signal 22: 398-410, 2015.
38. Zhang S, Yang G, Guan W, Li B, Feng X and Fan H: Autophagy plays a protective role in sodium hydrosulfide-induced acute lung injury by attenuating oxidative stress and inflammation in rats. Chem Res Toxicol 34: 857-864, 2021.
39. Chen L, Liu P, Feng X and Ma C: Salidroside suppressing LPS-induced myocardial injury by inhibiting ROS-mediated PI3K/Akt/mTOR pathway in vitro and in vivo. J Cell Mol Med 21: 3178-3189, 2017.
40. Wang C, Yuan W, Hu A, Lin J, Xia Z, Yang CF, Li Y and Zhang Z: Dexmedetomidine alleviated sepsis-induced myocardial ferroptosis and septic heart injury. Mol Med Rep 22: 175-184, 2020.
41. Ursini F and Maiorino M: Lipid peroxidation and ferroptosis: The role of GSH and GPX4. Free Radic Biol Med 152: 175-185, 2020.
42. Sun L, Dong H, Zhang W, Wang N, Ni N, Bai X and Liu N: Lipid peroxidation, GSH depletion, and SLC7A11 inhibition are common causes of EMT and ferroptosis in A549 cells, but different in specific mechanisms. DNA Cell Biol 40: 172-183, 2021.
43. Park E and Chung SW: ROS-mediated autophagy increases intracellular iron levels and ferroptosis by ferritin and transferrin receptor regulation. Cell Death Dis 10: 822, 2019.
44. Su LJ, Zhang JH, Gomez H, Murugan R, Hong X, Xu D, Jiang F and Peng ZY: Reactive oxygen species-induced lipid peroxidation in apoptosis, autophagy, and ferroptosis. Oxid Med Cell Longev 2019: 5080843, 2019.
45. Imai H, Matsuoka M, Kumagai T, Sakamoto T and Koumura T: Lipid peroxidation-dependent cell death regulated by GPx4 and ferroptosis. Curr Top Microbiol Immunol 403: 143-170, 2017.
46. Li J, Li M, Li L, Ma J, Yao C and Yao S: Hydrogen sulfide attenuates ferroptosis and stimulates autophagy by blocking mTOR signaling in sepsis-induced acute lung injury. Mol Immunol 141: 318-327, 2022.
47. Liang D, Minikes AM and Jiang X: Ferroptosis at the intersection of lipid metabolism and cellular signaling. Mol Cell 82: 2215-2227, 2022.
48. Gao M, Yi J, Zhu J, Yi J, Zhu J, Minikes AM, Monian P, Thompson CB and Jiang X: Role of mitochondria in ferroptosis. Mol Cell 73: 354-363.e3, 2019.
49. Fang X, Cai Z, Wang H, Han D, Cheng Q, Zhang P, Gao F, Yu Y, Song Z, Wu Q, *et al*: Loss of cardiac ferritin H facilitates cardiomyopathy via Slc7a11-mediated ferroptosis. Circ Res 127: 486-501, 2020.
50. He YJ, Liu XY, Xing L, Wan X, Chang X and Jiang HL: Fenton reaction-independent ferroptosis therapy via glutathione and iron redox couple sequentially triggered lipid peroxide generator. Biomaterials 241: 119911, 2020.
51. Li N, Wang W, Zhou H, Wu Q, Duan M, Liu C, Wu H, Deng W, Shen D and Tang Q: Ferritinophagy-mediated ferroptosis is involved in sepsis-induced cardiac injury. Free Radic Biol Med 160: 303-318, 2020.
52. Tang D, Chen X, Kang R and Kroemer G: Ferroptosis: Molecular mechanisms and health implications. Cell Res 31: 107-125, 2021.
53. Kuramoto K and He C: The secretory function of BECN1 in metabolic regulation. Autophagy 17: 3262-3263, 2021.
54. Hu F, Li G, Huang C, Hou Z, Yang X, Luo X, Feng Y, Wang G, Hu J and Cao Z: The autophagy-independent role of BECN1 in colorectal cancer metastasis through regulating STAT3 signaling pathway activation. Cell Death Dis 11: 304, 2020.
55. Lee S, Lee SJ, Coronata AA, Fredenburgh LE, Chung SW, Perrella MA, Nakahira K, Ryter SW and Choi AM: Carbon monoxide confers protection in sepsis by enhancing beclin 1-dependent autophagy and phagocytosis. Antioxid Redox Signal 20: 432-442, 2014.
56. Pi QZ, Wang XW, Jian ZL, Chen D, Zhang C and Wu QC: Melatonin alleviates cardiac dysfunction via increasing Sirt1-mediated beclin-1 deacetylation and autophagy during sepsis. Inflammation 44: 1184-1193, 2021.
57. Song X, Zhu S, Chen P, Hou W, Wen Q, Liu J, Xie Y, Liu J, Klionsky DJ, Kroemer G, *et al*: AMPK-mediated BECN1 phosphorylation promotes ferroptosis by directly blocking system X_c^- activity. Curr Biol 28: 2388-2399.e5, 2018.
58. Kang R, Zhu S, Zeh HJ, Klionsky DJ and Tang D: BECN1 is a new driver of ferroptosis. Autophagy 14: 2173-2175, 2018.
59. Yin Z, Ding G, Chen X, Qin X, Xu H, Zeng B, Ren J, Zheng Q and Wang S: Beclin1 haploinsufficiency rescues low ambient temperature-induced cardiac remodeling and contractile dysfunction through inhibition of ferroptosis and mitochondrial injury. Metabolism 113: 154397, 2020.
60. Liu R, Li X and Zhao G: Beclin1-mediated ferroptosis activation is associated with isoflurane-induced toxicity in SH-SY5Y neuroblastoma cells. Acta Biochim Biophys Sin (Shanghai) 51: 1134-1141, 2019.